Journal of Coastal Research	31	4	1005–1013	Coconut Creek, Florida	July 2015

REVIEW ARTICLES

www.cerf-jcr.org

Remote Sensing of Floods and Flood-Prone Areas: An Overview

Victor Klemas

School of Marine Science and Policy
University of Delaware
Newark, DE 19716, U.S.A.
klemas@udel.edu

www.JCRonline.org

ABSTRACT

Klemas, V., 2015. Remote sensing of floods and flood-prone areas: An overview. *Journal of Coastal Research,* 31(4), 1005–1013. Coconut Creek (Florida), ISSN 0749-0208.

River floods and coastal storm surges affect the lives of more people than most other weather-related disasters. Floods can destroy homes, roads, and bridges; tear out trees; cause mudslides; and take many human lives. During flooding, timely and detailed situation reports are required by disaster management authorities to locate and identify affected areas and to implement damage mitigation. Remote sensing systems on satellites and aircraft can provide much of the required information for delineating the flood-affected areas, assessing the damage, and feeding models that can predict the vulnerability to flooding of inland and coastal areas. In this article, I provide an overview of remote sensing and modeling techniques for forecasting the vulnerability to flooding of an area, determining the extent and intensity of the flooding, and assessing the damage caused by the flood.

ADDITIONAL INDEX WORDS: *Flood remote sensing, coastal flooding, storm surge, river flooding, flooding vulnerability, flood damage assessment.*

INTRODUCTION

In the long term, floods kill more people in the United States than other weather-related events. Floods can destroy buildings, roads, and bridges; tear out trees; devastate agriculture; cause mudslides; and threaten human lives (NOAA/NWS, 2005). Floods are difficult to monitor on large scales, because they are determined by local conditions such as precipitation, slope of terrain, drainage network, protective structures, land cover, and other factors. Each river or coastal area must be monitored at different places along its course. Some flood disasters happen annually, yet others can occur unexpectedly (De Groeve, 2010; Harman *et al*., 2014).

Once a river reaches flood stage, the flooding severity categories used by the National Weather Service (NWS) include minor flooding, moderate flooding, and major flooding. Minor flooding produces minimal or no property damage, but some public threat or inconvenience. Moderate flooding causes some inundation of structures and roads near streams, and some evacuation of people may be necessary. Major flooding causes extensive inundation of structures and roads, and significant evacuations of people and transfer of property to higher elevations may be required.

In the United States for each NWS river forecast location, flood stages associated with each of the NWS flood severity categories have been established in cooperation with local public officials. Increasing river levels above flood stage constitute minor, moderate, and major flooding. Effects vary from one river location to another, because a certain river stage (height) above flood stage in one location may have an entirely different effect than the same level above flood stage at another location (NOAA/NWS, 2005).

Flash floods are a serious danger for many people and develop when water rises rapidly along a stream or low-lying area. They are usually of short duration and with a relatively high peak discharge. Many people living on a flood plain are unaware of the danger they face, especially in urban settings (Coulibaly, 2008). Flash flood damage and most fatalities occur mainly in areas close to a stream or arroyo from a combination of heavy rain, dam break, levee failure, or rapid snowmelt. Flash floods are usually produced when slow-moving or multiple thunderstorms occur over the same area. When storms move faster, flash flooding is less likely because the rain is distributed over a broader area. Steep hills produce rapid runoff and quick stream response. Steep narrow valleys generate rapidly flowing waters that can rise quickly to a considerable depth (NOAA/NWS, 2005).

Seawater can inundate coasts in several different ways. Direct inundation occurs when sea height exceeds the elevation of the land, usually where there is no natural barrier such as a dune system. Natural or human-constructed barriers, such as levees, may be overtopped by swell conditions during storms or unusually high tides. Barriers may be breached, especially on

DOI: 10.2112/JCOASTRES-D-14-00160.1 received 20 August 2014; accepted in revision 26 September 2014; corrected proofs received 17 November 2014; published pre-print online 24 December 2014.

open stretches of the coast. As water flows over the top of the barrier, high-velocity flows can result that erode significant amounts of the land surface and undermine the defense barriers (Doorncamp, 1998; Ramsay and Bell, 2008; Wikipedia, 2014).

Coastal storm surges can cause major destruction and loss of life. Storm surges develop when water is pushed toward the shore by the force of a storm's wind. Horizontally, the surge can fan out over several hundred miles of coastline. In general, the more intense the hurricane and the closer a community to the right-front quadrant, the larger the area that must be evacuated. Vertically, the surge can reach heights of more than 6 m near the center of a Category 5 hurricane. Furthermore, the astronomical tide can add up to 1 m to the storm surge. Such a surge of high water, combined with high tides and torrential rains, in addition to battering waves, can be devastating to any coastal community (Harman *et al*., 2014; Klemas, 2009; Morton and Barras, 2011). In addition to urban communities and beaches, nearly 100,000 km of coastal roadways are in the 100-year floodplain in the United States, including many that are exposed to water surges and storm waves generated by hurricanes (Chen *et al.,* 2007; Harman *et al*., 2014).

For regional or nationwide use in coastal flood hazard analysis, attempts have been made to define a generic flood stage (FS) as an elevation at which significant flooding of local infrastructure is initiated (Kriebel and Geiman, 2014). By using monthly tidal gauge data from several coastal locations, a coastal FS based on the statistics of extreme high water events has been proposed. This statistical FS can then be compared with moderate and major FS values established by the NWS with good agreement. Once adopted, the FS would serve as a less ambiguous reference elevation or threshold to which the flooding potential of future storm events and sea level rise can be compared and would allow for consistent comparisons between different sites (Kriebel and Geiman, 2014).

Flooding and windstorms have been linked with climate change, and the number of disastrous floods and storms reported globally has tripled over the past three decades. Heavy precipitation has increased sharply in the last half century in many parts of the globe, including the Northeast and Midwest of the United States. Coastal communities in particular are facing a rising sea level, caused mainly by global warming (Church *et al*., 2010). A scientific consensus states that, as average temperatures increase worldwide, sea levels will continue to rise globally. Many scientists believe that because of melting glaciers and expanding ocean water, the sea level rise will accelerate in the future (IPCC, 2007). Since 1993, satellite observations have permitted more precise calculations of global sea level rise, now estimated to be 3.1 ± 0.7 mm/y over the period 1993–2003. The Intergovernmental Panel on Climate Change (IPCC) estimates global mean sea level rise from 1990 to 2100 to be between 9 and 88 centimeters. It also predicted that with climate change there may be an increase in the intensity and frequency of storm events such as hurricanes. Thus coastal flooding from storm surges may become more frequent with sea level rise (Cazenave and Llovel, 2010; Church *et al*., 2010).

The substantial sea level rise and more frequent storms predicted for the next 50–100 years would affect coastal cities and roads, coastal economic development, beach erosion control strategies, salinity of estuaries and aquifers, coastal drainage and sewage systems, and coastal wetlands (Cazenave and Llovel, 2010; Doorncamp, 1998; NOAA, 1999).

During flooding, timely and detailed situation reports are required by disaster management authorities to locate and identify the affected areas and to implement the required damage mitigation. This critical management function involves rescue operations and the safety of people and property (Haq *et al*., 2012; Ogashawara, Curtarelli, and Ferreira, 2013). Traditionally, coastal flooding due to hurricanes has been estimated by measured water levels on buoys and coastal gauges. Although these monitoring networks provide good historical data for coastal flooding, they lack spatial information because of the limited number of stations over many large areas. For the past few decades, optical and radar remote sensing systems on satellites and aircraft have been able to provide much of the required information for mapping the extent of a flood, assessing the damage, and feeding models that can evaluate the vulnerability to flooding of various inland and coastal areas.

The objective of this article is to provide an overview of remote sensing and modeling techniques that enable scientists and managers to evaluate the vulnerability of an area to flooding, determine the extent and intensity of the flooding, and assess the damage caused by the flooding event.

REMOTE SENSING OF FLOOD EXTENT

Conventional hydrological monitoring systems have limited use in flood forecasting, mapping, and emergency response. For large countries the cost of maintaining rain and stream gauging stations can be a limiting factor. Stations out of service can cause gaps in the hydrographic time series. Rivers are often shared between countries, but information on floods in upstream countries is not always communicated to downstream countries. For adequate flood warning, countries need to be able to collect information across borders independently. Furthermore, gauging stations measure water height, but not the extent of the flood. Remote sensors on satellites and aircraft can provide data to meet these requirements.

The availability of multitemporal satellite data allows monitoring flooding over large coastal areas. Aerial reconnaissance has been effective for determining the spatial extent of coastal and river flooding in detail for relatively small areas (Jensen, 2007; Klemas, 2013; Puech and Raclot, 2002; Webster *et al*., 2004). Aircraft equipped with state-of-the-art high-resolution digital cameras, like the ADS40, are often used for detailed mapping of flooded coastal areas or rivers. Generally, for flood mapping, two sets of remotely sensed data are required: one set comprising data acquired before the flood event and the other obtained during the flood occurrence (Wang, Colby, and Mulcahy, 2002). The image before the flood is usually used as a reference. These data can be used to map inundation areas and delineate flood boundaries. Field measurements can be integrated with remote sensing measurements from aircraft or satellites to observe changes in surface water extent and obtain other hydrologic information. River discharge estimates can be obtained using high-resolution

satellite data and a few ground measurements (Brivio *et al.*, 2002; Reid, Tissot, and Williams, 2014; Smith, 1997).

Optical Remote Sensing of Flood Extent

Both optical and microwave remote sensors are used in flood inundation monitoring. Optical sensors detect energy naturally reflected or emitted by the earth's surface in visible and infrared spectral bands. Where clouds, trees, and floating vegetation do not obscure the water surface, high-resolution visible/infrared sensors provide good delineation of inundated areas. Near-infrared imagers are especially effective, because the near-infrared spectral bands are strongly absorbed by water, yet reflected by land. In addition to airborne sensors, both medium-resolution (*e.g.*, Landsat Thematic Mapper [TM]) and high-resolution (*e.g.*, IKONOS) satellite multispectral sensors are used (Brivio *et al.*, 2002; Dewan, Kumamoto, Nishigaki, 2006; Frazier and Page, 2000; Hussain *et al.*, 2011; Jain *et al.*, 2005; Ngiem *et al.*, 2000; Sanyal and Lu, 2004; Wang, 2004). For example, Brakenridge and Anderson (2006) used Moderate-Resolution Imaging Spectroradiometer (MODIS) data for major flood detection, mapping, and measurement in the United States and Europe.

The Mississippi and Missouri River flood of 1993 presented a great opportunity to show the value of satellite sensors for mapping large flooded areas. The flood occurred along the two rivers and their tributaries from April to October of 1993 and became one of the most costly and devastating disasters, with tens of billions of dollars in damages and at least 32 fatalities. In St. Louis the river levels were nearly 6 m above flood stage. and the 16-m-high St. Louis Floodwall was able to keep the 1993 flood out with only 0.6 m to spare. NASA used the TM onboard the Landsat 5 satellite to map the flooded area during and before the flood. The image pair in Figure 1 shows the area around St. Louis, Missouri, on August 1991 and 1993, respectively (NASA/EO, 2005). The 1993 image was captured slightly after the peak water levels in this part of the Mississippi River. Flood waters had started to recede, but remained well above normal. These false color images were created by combining infrared, near infrared, and green wavelengths of light observed by the TM (bands 5, 4, and 2, respectively). In Figure 1, water is shown as dark blue, healthy vegetation is green, bare fields and freshly exposed soil are pink, and concrete is grey. The scale of flooding in the Illinois, Missouri, and Mississippi Rivers in 1993 was immense. The deep pink scars in the 1993 image show where flood waters have retreated to reveal the scoured land (NASA/EO, 2005).

Wang, Colby, and Mulcahy (2002) developed an efficient and economical approach for mapping flooding extent in a coastal floodplain. The method is based on the reflectance features of water *vs.* nonwater targets on a pair of Landsat 7 TM images obtained before and during the flood event, as well as modeling inundation using digital elevation model (DEM) data. Incorporation of the DEM data into the analysis was necessary because the TM data had difficulty detecting flooded areas beneath dense vegetation canopies, resulting in low flooded area numbers. The DEM data helped significantly in identifying the flooding that occurred underneath forest canopies, especially within bottomland forest and hardwood swamps. With the use of limited ground observations, most flooded and nonflooded areas derived from this analysis were verified. One of the limitations of integrating DEM data with TM data for flood mapping is that river gauge readings have to be used to inundate the DEM (Wang, Colby, and Mulcahy, 2002).

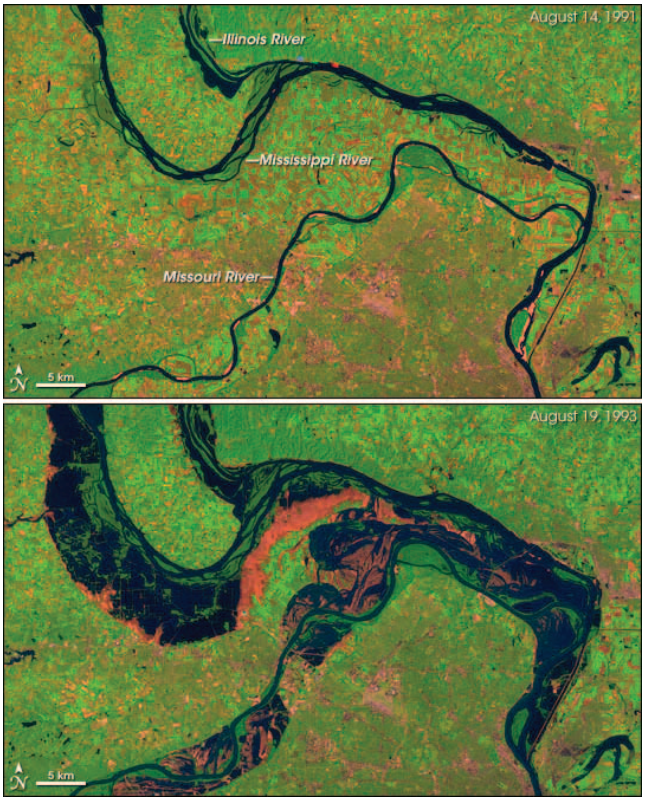

Figure 1. Landsat 5 TM false-color images of the 1993 Mississippi and Missouri flood. The upper image was taken in August 1991 (before the flood), and the lower image was obtained in August 1993 (during the flood). Water appears dark blue, healthy vegetation is green, bare fields and freshly exposed soil are pink, and concrete is grey. Viewing each image from the top down, the rivers are the Illinois, the Mississippi, and the Missouri. Credits: NASA Earth Observatory (NASA/EO, 2005).

A unique application of optical remote sensing for mapping flooded areas is presented by Ogashawara, Curtarelli, and Ferreira (2013). They used the Difference of Normalized Difference Water Indices (DNDWI) derived from two medium-resolution Landsat 5 TM surface reflectance products from the Landsat climate data record, acquired before and after the passage of Hurricane Ike through Texas in September 2008. They used as end members a classification of estimated flooded area based on the U.S. Geological Survey mobile storm surge network that was deployed for Hurricane Ike. A dataset consisting of 59 water level recording stations was used. The flooded areas were delineated using DNDWI with a threshold analysis method. A DEM was used for obtaining the topography of the region. The results showed that the difference of the DNDWI between flooded and unflooded areas was large enough to be exploited for mapping flooded areas. Mapping flooded areas with DNDWI gave an accuracy of 85.68%, whereas the unflooded areas had an accuracy of 92.13%. The authors

observe that additional spectral behavior studies are needed to explain the relationship between water content and vegetation spectral response in flooded areas.

Microwave Remote Sensing of Flood Extent

Active microwave sensors, such as synthetic aperture radar (SAR), provide their own illumination and record the amount of incident energy returned from the imaged surface. SAR can penetrate clouds, emergent aquatic plants, and forest canopies to detect standing water (Brivio *et al*., 2002; Horritt, Mason, and Luckman, 2001; Lawrence *et al*., 2005; Townsend, 2002). Cloud penetration is particularly important for monitoring flood events because they commonly occur during hurricane-related flooding or periods of extended rainfall (Kiage *et al*, 2005; Stevens, 2013; Townsend and Walsh, 1998). Discrimination of inundated areas can be optimized by selecting the most suitable polarization of the radar waves.

Henry *et al*. (2006) compared the Envisat advanced SAR (ASAR) with the performance of the SAR system on ERS-2 to evaluate the contribution of polarized configurations to flood boundary delineation. The ASAR instrument was activated in the alternating polarization and image modes, providing high-resolution data sets. They observed that HH polarization provides a more suitable discrimination of flooded areas than HV or VV. However, HV improved the existing HH data and proved to be an important contributor to flood detection. VV polarized data was highly influenced by surface roughness conditions.

Consequently, an alternating polarization precision image, using like- and cross-polarization, seemed to constitute a better image for flood mapping than a monopolarized image, especially if a rapid mapping response is required (Baghdadi *et al.,* 2001; Henry *et al*., 2006; Ngiem *et al.,* 2000). Ramsey *et al*. (2012) presented a summary of the limitations and potentials of satellite imagery to monitor and map coastal flooding for Hurricanes Gustav and Ike (2008), demonstrating that the correspondence between ground data and ASAR-based flood mapping ranged from 86% to 96% for water levels >0.8 m.

Some scientists have used both radar and optical remote sensors to monitor flood inundation. For example, Mallinis *et al*. (2011) developed and validated three object-based classification approaches using Envisat/ASAR and multitemporal Landsat TM data for flood area delineation. The accuracy assessment of the classification results was based on air photo interpretation and an area-based comparison with official flood maps. The bilevel object-based model using the normalized difference water index and the original postflood TM bands attained 92.67% overall accuracy in inundated area detection, whereas the Envisat/ASAR classification was the least accurate (85.33%), probably because of the lower spatial resolution of the ASAR image. Strong agreement (92.14%) was found between the Landsat flood extent and the official flood maps. The authors suggest that their method could be used in flood crisis management (Mallinis *et al*., 2011).

Radar altimeters can directly measure flood stage variations in large rivers (Calmant, Seyler, and Cretaux, 2008; Smith and Pavelsky, 2009). Satellite altimetry has also been used to investigate seasonal, interannual and space-time variability of the water levels of large lakes and coastal areas (Cazenave *et al*., 1997). Radar scatterometer data from satellites such as QuikSCAT have been used to detect changes in surface water area with frequent global coverage (Brakenridge *et al*., 2003). Airborne light detection and ranging (LIDAR) can determine water depths of inundated areas (Klemas, 2011).

De Groeve (2010) describes the use of passive microwave observations to detect, map, and size floods. Floods were detected as early as 2 hours after they occurred. Early warning was possible by monitoring upstream areas, with warning lead times up to 30 days. The flood maps were of low resolution but matched maps derived from high-resolution imagery. The daily availability of the data allowed a better understanding of the dynamics of the floods and objective flood sizing by integrating information over time and space. The results of this technique were used to study the 2009 floods in southern Africa and the 2010 flood season in Namibia (De Groeve, 2010).

FLOOD DAMAGE ASSESSMENT

Aerial photography has been used for >60 years to inspect flood damage to urban and coastal areas (Myers and Miller, 2005; Smith *et al*., 2007). For example, the flood damage caused by Hurricane Katrina in New Orleans in 2005 was mapped using a multidata approach, including airborne and satellite sensors (ASCE, 2007; Hill, 2012; Klemas, 2013; Waple, 2005). Satellite remote sensing techniques have expanded the scale for viewing flood damage and provide better identification of damage location and severity. For example, remotely sensed data has been used in a GIS to locate and identify flood-affected areas along with land use/land cover features. This method used processed satellite images that were then overlaid with population density data and land use/land cover maps for damage estimation. This approach required only a few hours and showed the capability to carry out rapid damage assessment (Haq *et al*., 2012).

Flood damage assessment can benefit from remote sensing imagery at both medium resolution (20–250 m) and high resolution (0.5–4 m). Medium-resolution imagery is used to assess the overall damage of flooding over large areas, such as coastal wetlands or entire city blocks, and can be obtained with satellite multispectral/hyperspectral or radar imagers (Gianinetto, Villa, and Lechi, 2006; Ramsey *et al*., 2012; Shan *et al*., 2009).

A good example of a medium-resolution application is presented in Figure 2, which shows an image of the Texas coast captured by the MODIS sensor on NASA's Terra satellite 13 days after Hurricane Ike made landfall on September 13, 2008. The storm's surge covered hundreds of kilometers of the Gulf Coast because Ike was a large storm, with tropical storm–strength winds stretching more than 400 km from the center of the storm. Most of the shoreline in this region is coastal wetland. One can clearly distinguish the red-brown areas on land, which are the result of the massive storm surge that Ike pushed far inland over Texas and Louisiana, causing a major marsh dieback. The salty water burned the plants, leaving them wilted and brown. In Figure 2, the brown line corresponds with the location and extent of the wetlands. North of the brown line, the vegetation gradually transitions to pale green farmland and dark green natural vegetation untouched by the

Figure 2. The moderate-resolution imaging spectroradiometer (MODIS) on NASA's Terra satellite captured this image on September 26, 2008, 13 days after Hurricane Ike came ashore. The brown areas in the image are the result of a massive storm surge that Ike pushed far inland over Texas and Louisiana, causing a major marsh dieback. Credits: NASA (NASA/GSFC, 2010).

storm's surge. The powerful tug of water returning to the Gulf also stripped marsh vegetation and soil off the land. Therefore, some of the brown seen in the wetlands may be deposited sediment. Plumes of brown water are visible as sediment-laden water drains from rivers and the coast in general. The muddy water slowly diffuses, turning pale green, green, and finally blue as it blends with clearer Gulf water (NASA/GSFC, 2010; Ramsey and Rangoonwala, 2005).

To map the flooding in New Orleans and its vicinity caused by hurricane Katrina, a multidata base approach was used (ASCE, 2007; Klemas, 2009; Wikipedia, 2008). The map was created by incorporating SAR and other images acquired during the flood with a preflood Landsat-enhanced TM image mosaic. The ability of SAR to penetrate clouds and vegetation cover made it quite useful for flood mapping. Also, SAR provided information on urban damage that complemented the spectral information from optical multispectral imagers, such as Landsat TM and other satellites. The Landsat TM and other remotely sensed images gave emergency managers and coastal engineers a clear view of inundated areas and helped plan pumping and other recovery efforts.

High-resolution imagery provided by airborne cameras or high-resolution satellite imagers is used to determine the detailed damage to structures such as houses, roads, and levees (Table 1). For example, sections of levees designed to channel canals through New Orleans crumbled under the battering waves and storm surge of hurricane Katrina. The breaks allowed water to flow from Lake Pontchartrain into New Orleans, inundating the city (Hill, 2012). The levee breaks, with water rushing into the city, could clearly be seen in high-resolution satellite imagery, such as IKONOS and QuickBird (Table 1). On August 31, 2005, the QuickBird satellite captured images of two levee breaks, as shown in Figure 3. The top image shows the 240-m-long breach in the levee along the Industrial Canal in East New Orleans. Water is pouring through a break in the canal in the lower half of the image. The streets on the opposite side of the Industrial Canal are also flooded, because of similar breaches in canals to the west.

The lower image in Figure 3 shows the 145-m-long breach in the 17th Street Canal in West New Orleans. Water is flooding the areas on the east side of the canal (top), but not the west side (bottom). The enlarged version of this image also shows widespread debris scattered across dry areas. Satellites, aircraft, and helicopters provided valuable imagery showing damaged bridges, highways, port facilities, oil rigs, and other coastal infrastructure (Digital Globe, 2009; Hill, 2012; NASA, 2005). To assess the hurricane damage to the levee system, the Army Corps of Engineers used topographic data obtained with a helicopter-mounted LIDAR sensor over the hurricane protection levee system in Louisiana. This information was very valuable for planning specific repairs and general reconstruction efforts.

Table 1. *High-resolution satellite parameters and spectral bands (DigitalGlobe, 2009; Orbimage, 2003; Parkinson, 2003; Space Imaging, 2003). n/a =not available.*

	IKONOS	QuickBird	OrbView-3	WorldView-1	GeoEye-1	WorldView-2
Sponsor	Space Imaging	DigitalGlobe	Orbimage	DigitalGlobe	GeoEye	DigitalGlobe
Launched	September 1999	October 2001	June 2003	September 2007	September 2008	October 2009
Spatial resolution (m)						
Panchromatic	1.0	0.61	1.0	0.5	0.41	0.5
Multispectral	4.0	2.44	4.0	n/a	1.65	2
Spectral range (nm)						
Panchromatic	525–928	450–900	450–900	400–900	450–800	450–800
Coastal blue	n/a	n/a	n/a	n/a	n/a	400–450
Blue	450–520	450–520	450–520	n/a	450–510	450–510
Green	510–600	520–600	520–600	n/a	510–580	510–580
Yellow	n/a	n/a	n/a	n/a	n/a	585–625
Red	630–690	630–690	625–695	n/a	655–690	630–690
Red edge	n/a	n/a	n/a	n/a	n/a	705–745
Near infrared	760–850	760–890	760–900	n/a	780–920	770–1040
Swath width (km)	11.3	16.5	8	17.6	15.2	16.4
Off-nadir pointing	±26°	±30°	±45°	±45°	±30°	±45°
Revisit time (d)	2.3–3.4	1–3.5	1.5–3	1.7–3.8	2.1–8.3	1.1–2.7
Orbital altitude (km)	681	450	470	496	681	770

Figure 3. QuickBird satellite images of New Orleans levee breaks. The top image shows a 240-m-long breach in levees along the Industrial Canal through which water is pouring. The lower image shows a 145-m-long breach in the 17th Street Canal flooding the areas on the east side of the canal (top), but the west side (bottom) remains dry (Digital Globe, 2009).

ASSESSING VULNERABILITY TO FLOODING

Accurate determination of vulnerability to flooding is critical to habitat conservation, littoral boundary definition, and coastal protection planning. Flood vulnerability prediction systems can also help mitigate a variety of flood-induced hazards. Typically such systems require implementation and calibration of a hydrologic model using *in situ* observations (*i.e.* rain and stream gauges). The output of a typical hydrodynamic model provides georeferenced predictions that can be used to delineate a wet/dry boundary (Li, Lin, and Burks-Copes, 2013; Mason, Bates, and Amico, 2009; Reid, Tissot, and Williams, 2014; Townsend and Walsh, 1998).

The use of satellite remote sensing data in a model can supplement *in situ* observations over vast ungauged regions, delineate the extent of flooding, and identify areas vulnerable to future flooding (Islam and Sado, 2002; Schumann et al., 2009; Van Alphen *et al*., 2009). For example, Khan *et al*. (2011) implemented a raster-based distributed hydrologic model, coupled routing and excess storage (CREST) for the Nzoia basin, a subbasin of Lake Victoria in Africa. Terra satellite–based MODIS data and advanced spaceborne thermal emission and reflection radiometer (ASTER) data were used to produce flood inundation maps over the region. The maps were used to benchmark the distributed hydrologic model simulations of inundation areas. The analysis showed the value of integrating satellite data such as precipitation, land cover type, topography, and other products with space-based flood inundation extents as inputs to the distributed hydrologic model. The results confirmed that the quantification of flooding extent through remote sensors can help to calibrate and evaluate hydrologic models and, therefore, improve hydrologic prediction and flood management strategies, especially in poorly gauged catchments (Khan *et al*., 2011).

In coastal areas, storm-induced flooding and other damage present a major problem because the coastal population continues to increase rapidly and the sea level keeps rising. For flood risk mapping from storm surge events, scientists have used high-resolution satellite imagery and airborne LIDAR data (Webster *et al*., 2004, 2006). A typical model used by the National Oceanic and Atmospheric Administration (NOAA) National Hurricane Center to estimate storm surge heights and winds resulting from predicted or hypothetical hurricanes is the sea, lake, and overland surges from hurricanes (SLOSH) model. It takes into account the pressure, size, forward speed, track, and winds of a hurricane. SLOSH is used to evaluate the threat from storm surges, and emergency managers use these data to determine which areas must be evacuated. SLOSH model results are combined with road network and traffic flow information, rainfall amounts, river flow, and wind-driven waves to identify at-risk areas (NOAA/CSC, 2008).

The dynamical SLOSH model computes water height over a geographical area or basin. The calculations are applied to a specific locale's shoreline, incorporating the unique bay and river configurations, water depths, bridges, roads, and other physical features. Computations have been run for a number of basins covering most of the Atlantic and Gulf Coasts of the United States and offshore islands. The typical SLOSH grid contains more than 500 points located on lines extending radially from a common basin center. The distance between grid points ranges from 0.5 km near the center (where surge water heights are of more interest) to 7.7 km in the deep water at the edge of the grid. Bathymetric and topographic map data are used to determine a water depth or terrain height for each grid point. The model consists of a set of equations derived from the Newtonian equations of motion and the continuity equation applied to a rotating fluid with a free surface. The equations are integrated from the sea floor to the sea surface. The coastline is represented as a physical boundary within the model domain. Subgrid-scale water features (cuts, chokes, sills, and channels) and vertical obstructions (levees, roads, spoil banks, *etc*.) can be parameterized within the model. Astronomical tides, rainfall, river flow, and wind-driven waves have not been incorporated into the model (NOAA/CSC, 2008).

The primary use of the SLOSH model is to define flood-prone areas for evacuation planning. The flood areas are determined by compositing the model surge values from 200 to 300 hypothetical hurricanes. Separate composite flood maps are produced for each of the five Saffir-Simpson hurricane categories. The SLOSH model can also be run with forecast track and intensity data for a storm as it makes landfall.

Many other flood forecasting and flood risk management models are being used by commercial firms and government agencies. For example, the advanced Hurricane Storm Surge Risk model from CoreLogic provides coastal risk management by combining four datasets—storm surge flooding risk, distance to coast, evacuation zones, and mainland configuration. Even small companies can access the coastal risk data layers, as well as other natural hazard risk assessments, through a simple desktop system (Anonymous, 2014).

Sea level rise is expected to affect natural and urban areas by shifting habitats and inundating infrastructure. Thus, it is important to identify human and ecological vulnerabilities to sea level rise. One of the models used to simulate the effects on urban, developed lands, and environmental systems from sea level rise is the sea level affecting marshes model (SLAMM). It can be used to simulate land cover and land use change through wetland migration under various sea level rise scenarios (*e.g.*, sea level rises of 0.25, 0.50, 0.75, and 1.00 m in magnitude). SLAMM predictions are being used for sustainable planning under predicted climate conditions in the future (Linhoss *et al.*, 2014).

Validating a hydrodynamic model against field observations is essential for evaluating model performance. Reid, Tissot, and Williams (2014) present two geospatial methods that complement *in situ* point-based validation. The methods utilize the coastal modeling system (CMS) hydrodynamic model and ArcMap software. The techniques are applicable to calibrated hydrodynamic models and can be applied independently or together. Each method was validated with an extensive data set available for tidal flats located along the Packery Channel, Texas. The first method compared model predictions to the observed conditions of high-resolution satellite and aerial imagery, which were classified using one of two geospatial processes. The second method applied the model output to delineate the maximum flood extent and then compared the predicted extent to topographic surveys, which define the true time-dependent flood line. Analyses showed agreement between model predictions and classified imagery ranging from 69% to 91%. These methodologies expand capabilities to assess and improve hydrodynamic model predictions, particularly for delineating inundation in shallow coastal environments (Reid, Tissot, and Williams, 2014).

SUMMARY AND CONCLUSIONS

Floods are among the most destructive natural disasters around the globe affecting human lives and infrastructure. During flooding, timely and detailed situation reports are required by disaster management authorities to identify and map the affected areas and to implement the required damage mitigation. This is a critical management function because it involves rescue operations and the safety of people and property. Floods are difficult to monitor on large scales because they are determined by local conditions such as precipitation, slope of terrain, drainage network, protective structures, land cover, and other factors. Conventional hydrological monitoring systems during floods have limited use for flood forecasting, mapping, and emergency response. Gauging stations measure the water height, but not the extent of the flood. Furthermore, maintaining a multitude of gauging stations can be a limiting factor.

Optical and radar remote sensing systems on satellites and aircraft have been able to provide much of the required information for observing and delineating the flood-affected areas, assessing the damage, and feeding models that can evaluate the vulnerability to flooding of various inland and coastal areas. These data can be used to map inundation areas and delineate flood boundaries across national borders. Field measurements can be integrated with remote sensing data from aircraft or satellites to observe changes in surface water extent and obtain other hydrologic information.

Where clouds and trees do not obscure the water surface, high-resolution visible/infrared sensors provide good delineation of coastal inundated areas. Near-infrared imagers are especially effective because near-infrared spectral bands are strongly absorbed by water, yet reflected by land. Active sensors, such as SAR, can penetrate clouds, emergent aquatic plants, and forest canopies to detect standing water. Radar altimeters can directly measure river stage variations in large rivers. Airborne LIDAR can be used to determine water depths of inundated areas.

Flood damage assessment can benefit from remote sensing imagery at both medium resolution (20–250 m) and high resolution (0.5–4 m). Medium-resolution imagery is used to assess the overall damage of flooding over large areas, such as coastal wetlands or entire city blocks, and can be obtained with satellite multispectral/hyperspectral or radar imagers. High-resolution imagery is used to determine the detailed damage to houses, roads, levees, and other structures and is provided by airborne cameras or high-resolution satellite imagers.

Flood vulnerability prediction systems help mitigate flood-induced hazards. Typically such systems require implementation and calibration of a hydrologic model using *in situ* observations (*i.e.* rain and stream gauges). Using satellite remote sensing data in a model can supplement *in situ* observations over vast ungauged regions and delineate the extent of the flooding. Mapping the spatial extent of flooding through remote sensors helps calibrate and evaluate hydrologic models and, therefore, improve hydrologic prediction and flood management strategies, especially in poorly gauged catchments.

Storm-induced coastal flooding presents a major problem as the coastal population continues to increase and the sea level keeps rising. A practical model used by the NOAA National Hurricane Center to estimate storm surge heights and winds resulting from predicted or hypothetical hurricanes is the SLOSH model. It takes into account the pressure, size, forward speed, track, and winds of a hurricane. SLOSH is used to evaluate the threat from storm surges, and emergency managers use these data to determine which areas must be evacuated. SLOSH model results are combined with road network and traffic flow information, rainfall amounts, river flow, and wind-driven waves to identify at-risk areas.

In summary, remotely sensed data are increasingly being used for flood extent mapping, damage assessment and vulnerability prediction. Optical sensor data are readily available at reasonable cost for extended areas and can be used with available well-defined, robust data processing

techniques. Optical sensors cannot penetrate clouds or vegetation cover. Effective and timely flood warning can be attained with frequent radar observations of flood-prone areas through cloud cover. However, radar data can be more expensive and more difficult to interpret and analyze.

LITERATURE CITED

Anonymous, 2014. Coastal risk and storm surge tool improves risk management. *Environment Coastal and Offshore,* September 2014, 51.

ASCE (American Society of Civil Engineers) Staff, 2007. The New Orleans Hurricane Protection System: What Went Wrong and Why. Reston, Virginia: American Society of Civil Engineers, *Report of the ASCE Hurricane Katrina External Review Panel*, 92p.

Baghdadi, N.; Bernier, M.; Gauthier, R., and Neeson, I., 2001. Evaluation of C-band SAR data for wetlands mapping. *International Journal of Remote Sensing*, 22(1), 71–88.

Brakenridge, G.R. and Anderson, E., 2006. MODIS-based flood detection, mapping and measurement: The potential for operational hydrological applications. In: Marsalek, J.; Stancalie. G., and Balint, G., (eds.), *Transboundary Floods: Reducing Risks through Flood Management*. NATO Science Series IV: Earth and Environmental Sciences, Volume 72. Cham, Switzerland: Springer, pp. 1–12.

Brakenridge, G.R.; Anderson, E.; Nghiem, S.V.; Caquard, S., and Shabaneh, T.B., 2003. Flood warnings, flood disaster assessments, and flood hazard reduction: The roles of orbital remote sensing. *Proceedings of the 30th International Symposium on Remote Sensing of Environment* (Honolulu, Hawaii, International Center for Remote Sensing of Environment), 6p.

Brivio, P.A.; Colombo, R.; Maggi, R., and Tomasoni, R., 2002. Integration of remote sensing data and GIS for accurate mapping of flooded areas. *International Journal of Remote Sensing,* 23(3), 429–441.

Calmant, S.; Seyler, F., and Cretaux, J.F., 2008. Monitoring continental surface waters by satellite altimetry. *Surveys in Geophysics*, 29(4–5), 247–269.

Cazenave, A.; Bonnefond, P.; Dominh, K., and Schaeffer, P., 1997. Caspian sealevel from TOPEX-POSEIDON altimetry: Level now falling. *Geophysical Research Letters,* 24(8), 881–884.

Cazenave, A. and Llovel, W., 2010. Contemporary sea level rise. *Annual Review of Marine Science,* 2(January), 145–173.

Chen, Q.; Wang, L.; Zhao, H., and Douglass, S.L., 2007. Prediction of storm surges and wind waves on coastal highways in hurricane-prone areas. *Journal of Coastal Research,* 23(5), 1304–1317.

Church, J.A.; Woodworth, P.L.; Aarup, T., and Wilson, W.S. (eds.), 2010. *Understanding Sea-Level Rise and Variability*. 1st edition. Oxford, U.K.: Blackwell, 454p.

Coulibaly, M., 2008. Spatial analysis of an urban flash flood results. *Geocarto International,* 23(3), 217–234.

De Groeve, T., 2010. Flood monitoring and mapping using passive microwave remote sensing in Namibia. *Geomatics, Natural Hazards and Risk*, 1(1), 19–35.

Dewan, M.A.; Kumamoto, T., and Nishigaki, M., 2006. Flood hazard delineation in greater Dhaka, Bangladesh using an integrated GIS and remote sensing approach. *Geocarto International,* 21(2), 33–38.

Digital Globe, 2009. *QuickBird*. http://www.digitalglobe.com.

Doorncamp, J.C., 1998. Coastal flooding, global warming and environmental management. *Journal of Environmental Management*, 52(4), 237–333.

Frazier, P.S. and Page, K.J., 2000. Water body detection and delineation with Landsat TM data. *Photogrammetric Engineering and Remote Sensing*, 66(12), 257–266.

Gianinetto, M.; Villa, P., and Lechi, G., 2006. Post-flood damage evaluation using Landsat TM and ETM+ data integrated with DEM. *IEEE Transactions on Geoscience and Remote Sensing*, 44(1), 236–243.

Haq, M.; Akhtar, M.; Muhammad, S.; Paras, S., and Rahmatullah, J., 2012. Techniques of remote sensing and GIS for flood monitoring and damage assessment: A case study of Sindh province, Pakistan. *The Egyptian Journal of Remote Sensing and Space Sciences,* 15(2), 135–141.

Harman, B.P.; Heyenga, S.; Taylor, B.M., and Fletcher, C.S., 2014. Global lessons for adapting coastal communities to protect against storm surge inundation. *Journal of Coastal Research*. In press. doi:10.2112/JCOASTRES-D-13-00095.1

Henry, J-B.; Chastanet, P.; Fellah, K., and Desnos, Y.-L., 2006. Envisat multipolarized ASAR for flood mapping. *International Journal of Remote Sensing*, 27(10), 1921–1929.

Hill, D., 2012. The lessons of Katrina: Learned and unlearned. *Journal of Coastal Research,* 28(2), 324–331.

Horritt, M.S.; Mason, D.C., and Luckman, A.J., 2001. Flood boundary delineation from Synthetic Aperture Radar imagery using a statistical active contour model. *International Journal of Remote Sensing*, 22(13), 2489–2507.

Hussain, E.; Ural, S.; Malik, A., and Shan, J., 2011. Mapping Pakistan 2011 floods using remote sensing. *Proceedings of the ASPRS 2011 Annual Conference* (Milwaukee, Wisconsin, American Society for Photogrammetry and Remote Sensing), 8p.

IPCC (Intergovernmental Panel on Climate Change), 2007. *Climate Change 2007: The Physical Science Basis*. Paris: WMO/UNEP. http://www.ipcc.ch.

Islam, M.M. and Sado, K., 2002. Development of priority map for flood countermeasure by remote sensing data with Geographic Information System. *Journal of Hydrologic Engineering,* 7(5), 346–355.

Jain, S.K.; Singh, R.D.; Jain, M.K., and Lohani, A.K., 2005. Delineation of flood-prone areas using remote sensing techniques. *Water Resources Management*, 19(4), 333–347.

Jensen, J.R., 2007. *Remote Sensing of the Environment: An Earth Resource Perspective*. New Jersey: Prentice-Hall, 592p.

Khan, S.I.; Hong, Y.; Wang, J.; Yilmaz, K.K.; Gourley, J.J.; Adler, R.F.; Brakenridge, G.R.; Policelli, F.; Habib, S., and Irwin, D., 2011. Satellite remote sensing and hydrologic modeling for flood inundation mapping in Lake Victoria basin: Implications for hydrologic prediction in ungauged basins. *IEEE Transactions on Geoscience and Remote Sensing*, 49(1), 85–95.

Kiage, L.M.; Walker, N.D.; Balasubramanian, S.; Babin, A., and Barras, J., 2005. Application of Radarsat-1 synthetic aperture radar imagery to assess hurricane-related flooding of coastal Louisiana. *International Journal of Remote Sensing*, 26(24), 5359–5380.

Klemas, V., 2009. The role of remote sensing in predicting and determining coastal storm impacts. *Journal of Coastal Research* 25(6): 1264–1275.

Klemas, V., 2011. Beach profiling and LIDAR bathymetry: An overview with case studies. *Journal of Coastal Research*, 27(6), 1019–1028.

Klemas, V., 2013. Airborne remote sensing of coastal features and processes: An overview. *Journal of Coastal Research*, 29(2), 239–255.

Kriebel, D.L. and Geiman, J.D., 2014. A coastal flood stage to define existing and future sea-level hazards. *Journal of Coastal Research*, 30(5), 1017–1024.

Lawrence, M.K.; Walker, N.D.; Balasubramanian, S., and Baras, J., 2005. Application of Radarsat-1 synthetic aperture radar imagery to assess hurricane-related flooding of coastal Louisiana. *International Journal of Remote Sensing*, 26(24), 5359–5380.

Li, H.; Lin, L., and Burks-Copes, K.A., 2013. Modeling of coastal inundation, storm surge, and relative sea-level rise at Naval Station Norfolk, Norfolk, Virginia, U.S.A. *Journal of Coastal Research,* 29(1), 18–30.

Linhoss, A.C.; Kiker, G.; Shirley, M., and Frank, K., 2014. Sea-level rise, inundation, and marsh migration: Simulating impacts on developed lands and environmental systems. *Journal of Coastal Research*. In press. doi:10.2112/JCOASTRES-D-13-00215.1

Mallinis, G.; Gitas, I.Z.; Giannakopoulos, V.; Maris, F., and Tsakiri-Strati, M., 2011. An object-based approach for flood area delineation in a transboundary area using ENVISAT ASAR and LANDSAT TM data. *International Journal of Digital Earth*, 6(2), S124–S136.

Mason, D.C.; Bates, P.D., and Amico, J.T., 2009. Calibration of uncertain flood inundation models using remotely sensed water levels. *Journal of Hydrology*, 368(1–4), 224–236.

Morton, R.A. and Barras, J.A., 2011. Hurricane impacts on coastal wetlands: A half-century record of storm-generated features from southern Louisiana. *Journal of Coastal Research*, 27(6A), 27–43.

Myers, J.S. and Miller, R.L., 2005. Optical airborne remote sensing. *In:* Miller, R.L.; Del Castillo, C.E., and Mckee, B.A. (eds.), *Remote Sensing of Coastal Aquatic Environments*. Dordrecht, The Netherlands: Springer, pp. 51–67.

NASA (National Aeronautics and Space Administration), 2005. *EO Natural Hazards: Hurricane Katrina floods the Southeastern United States*. http://earthobservatory.nasa.gov/NaturalHazards/view.php?id=15441.

NASA/EO (Earth Observatory), 2005. *Great flood of the Mississippi River, 1993*. http://earthobservatory.nasa.gov/IOTD/view.php?id=5422

NASA/GSFC (Goddard Space Flight Center), 2010. Hurricane Ike: storm surge flooding image of the Gulf Coast. NASA image courtesy Jeff Schmaltz, MODIS Rapid Response Team at NASA GSFC.

Ngiem, S.V.; Liu, W.T.; Tsai, W.-Y., and Xie, X., 2000. Flood mapping over the Asian continent during the 1999 summer monsoon season. *Proceedings of the IGARSS '00* (Honolulu, Hawaii, IEEE), pp. 2017–2028.

NOAA (National Oceanic and Atmospheric Administration), 1999. Trends in U.S. coastal regions, 1970–1998. *Addendum to the Proceedings: Trends, and Future Challenges for U.S. National Ocean and Coastal Policy*. (Washington, D.C., NOAA), 39p.

NOAA/NHC, 2014. *Sea, Lake, and Overland Surges from Hurricanes (SLOSH)*. NOAA National Weather Service National Hurricane Center. http://www.nhc.noaa.gov/surge/slosh.php.

NOAA/NWS (National Weather Service), 2005. Floods: The Awesome Power. *U.S. Department of Commerce, ARC 4493, NOAA PA 2000467*, 16p.

Ogashawara, I.; Curtarelli, M.P., and Ferreira, C.M., 2013. The use of optical remote sensing for mapping flooded areas. *International Journal of Engineering Research and Application,* 3(5), 1–5.

Orbimage, 2003. *OrbView-3 Satellite and Ground Systems Specifications*. Dulles, Virginia: Orbimage.

Parkinson, C.L., 2003. Aqua: An Earth-observing satellite mission to examine water and other climate variables. *IEEE Transactions on Geoscience and Remote Sensing,* 41(2), 173–183.

Puech, C. and Raclot, D., 2002. Using geographical information systems and aerial photographs to determine water levels during floods. *Hydrological Processes*, 16(8), 1593–1602.

Ramsay, D. and Bell, R., 2008. Coastal Hazards and Climate Change. A Guidance Manual for Local Government in New Zealand. 2nd edition. Wellington, New Zealand: National Institute of Water and Atmospheric Research (NIWA) and Ministry for the Environment.

Ramsey, E. and Rangoonwala, A., 2005. Leaf optical property changes associated with the occurrence of *Spartina alterniflora* dieback in coastal Louisiana related to remote sensing mapping. *Photogrammetric Engineering and Remote Sensing*, 71(3), 299–311.

Ramsey, E.; Werle, D.; Suzuoki, Y.; Rangoonwala, A., and Lu, Z., 2012. Limitations and potential of satellite imagery to monitor environmental response to coastal flooding. *Journal of Coastal Research,* 28(2), 457–476.

Reid, S.K.; Tissot, P.E., and Williams, D.D., 2014. Methodology for applying GIS to evaluate hydrologic model performance in predicting coastal inundation. *Journal of Coastal Research*, 30(5), 1055–1065.

Sanyal, J. and Lu, X.X., 2004. Application of remote sensing in flood management with special reference to monsoon Asia: A review. *Natural Hazards*, 33, 283–301.

Schumann, G.; Bates, P.D.; Horritt, M.S.; Matgen, P., and Pappenberger, F., 2009. Progress in integration of remote sensing-derived flood extent and stage data and hydraulic models. *Reviews of Geophysics*, 47(4), RG4001.

Shan, J.; Hussain, K.; Kim, K., and Biehl, L., 2009. Flood mapping and damage assessment—A case study in the state of Indiana. *In:* Li, D.; Shan, J., and Gong, J. (eds.), *Geospatial Technology for Earth Observation*. Dordrecht, The Netherlands: Springer, Chapter 18, pp. 473–495.

Smith, G.M.; Thomson, A.G; Wilson, A.K.; Hill, R.A., and Purcell, P.W., 2007. Airborne remote sensing for monitoring the impact of coastal zone management. *International Journal of Remote Sensing,* 28(7–8), 1433–1435.

Smith, L.C., 1997. Satellite remote sensing of river inundation area, stage, and discharge: A review. *Hydrological Processes*, 11, 1427–1439.

Smith, L.C. and Pavelsky, T.M., 2009. Remote sensing of volumetric storage changes in lakes. *Earth Surface Processes and Landforms*, 34, 1353–1358.

Space Imaging, 2003. *IKONOS Imagery Products and Product Guide* (version 1.3). Thornton, Colorado: Space Imaging.

Stevens, T.B., 2013. Synthetic aperture radar for coastal flood mapping. *NASA Global Change Master Directory*. Data Originator: LSU Earth Scan Laboratory, Baton Rouge. http://www.esl.lsu.edu/home/

Townsend, P.A., 2002. Relationship between forest structure and the detection of flood inundation in forested wetlands using C-band SAR. *International Journal of Remote Sensing,* 23(3), 443–460.

Townsend, P.A. and Walsh, S.J., 1998. Modeling floodplain inundation using an integrated GIS with radar and optical remote sensing. *Geomorphology*, 21(3–4), 295–312.

Van Alphen, J.; Martini, F.; Loat, R.; Slomp, R., and Passchier, R., 2009. Flood risk mapping in Europe, experiences and best practices. *Journal of Flood Risk Management*, 2(4), 285–292.

Wang, Y., 2004. Using Landsat 7 TM data acquired days after a flood event to delineate the maximum flood extent on a coastal floodplain. *International Journal of Remote Sensing*, 25(5), 959–974.

Wang, Y.; Colby, J.D., and Mulcahy, K.A., 2002. An efficient method for mapping flood extent in a coastal flood plain using Landsat TM and DEM data. *International Journal of Remote Sensing,* 23(18), 3681–3696.

Waple, A., 2005. *Hurricane Katrina*. NOAA's National Climatic Data Center, Asheville, North Carolina. http://www.ncdc.noaa.gov/extremeevents/specialreports/Hurricane-Katrina.pdf.

Webster, T.L.; Forbes, D.L.; Dickie, S., and Shreenan, R., 2004. Using topographic lidar to map flood risk from storm-surge events for Charlottetown, Prince Edward Island, Canada. *Canadian Journal of Remote Sensing*, 30(1), 64–76.

Webster, T.L.; Forbes, D.L.; MacKinnon, E., and Roberts, D., 2006. Flood risk mapping for storm-surge events and sea-level rise using lidar for southeast New Brunswick. *Canadian Journal of Remote Sensing,* 32(2), 194–211.

Wikipedia, 2008. *Hurricane Katrina*. http://en.wikipedia.org/wiki/Hurricane_Katrina.

Wikipedia, 2014. *Coastal Flood*. http://en.wikipedia.org/wiki/Coastal_flood.